Supplementary Information for

Cation Concentration-Dependent Reaction Kinetics in Single-Atom Catalysts for Electrochemical CO_2 Reduction

Lingyi Kong,[a] Zhe Chen,[a] Yuheng Chen,[a] Lingxiao Wang,[*,a] Yu Wang[a] and Yafei Li[*,a]

[a]Jiangsu Collaborative Innovation Center of Biomedical Functional Materials, Jiangsu Key Laboratory of New Power Batteries, School of Chemistry and Materials Science, Nanjing Normal University, Nanjing 210023, China.

*To whom correspondence should be addressed. Email: lxwang46@nnu.edu.cn; liyafei@njnu.edu.cn

Supplementary Figures

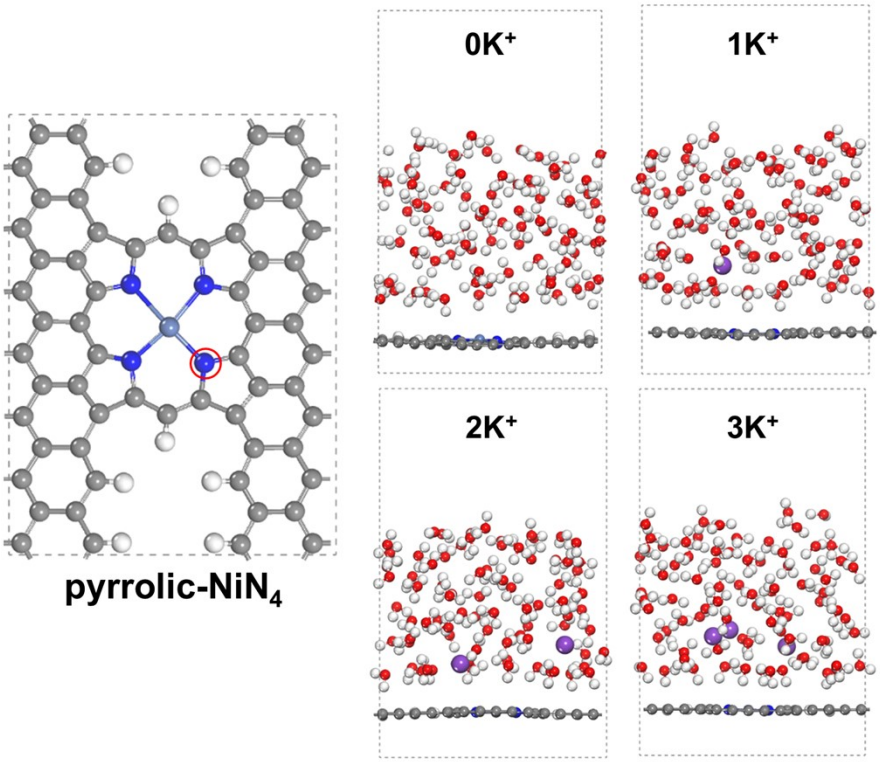

Fig. S1. Atomic structures of pyrrolic-NiN_4 with different solvent microenvironments. Gray, white, blue, indigo, red, and purple balls represent C, H, N, Ni, O, and K atoms, respectively.

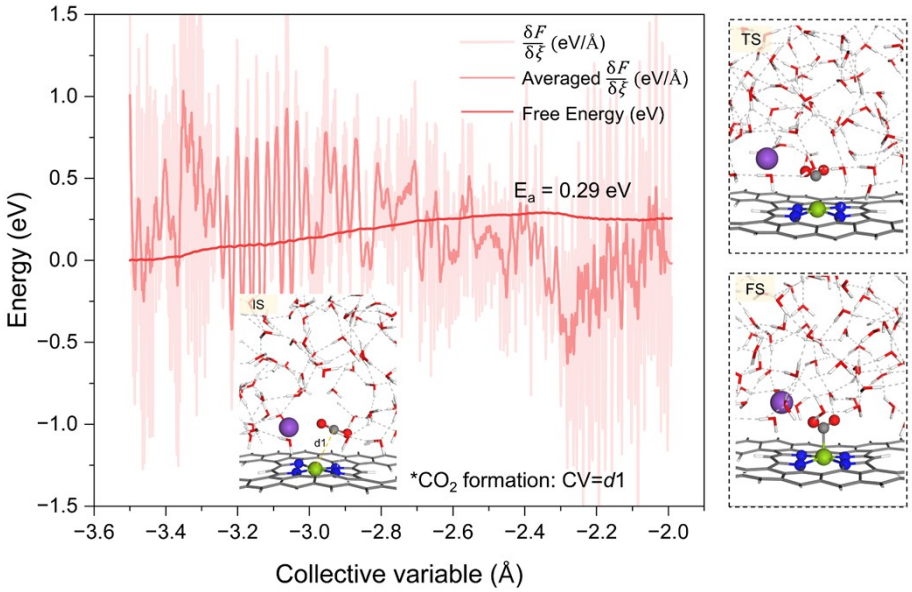

Fig. S2. Free energy profiles for CO_2 adsorption under $1K^+$ condition. The insert is the view of the initial state (IS) while the views of the transition state (TS) and final state (FS) are displayed on the right.

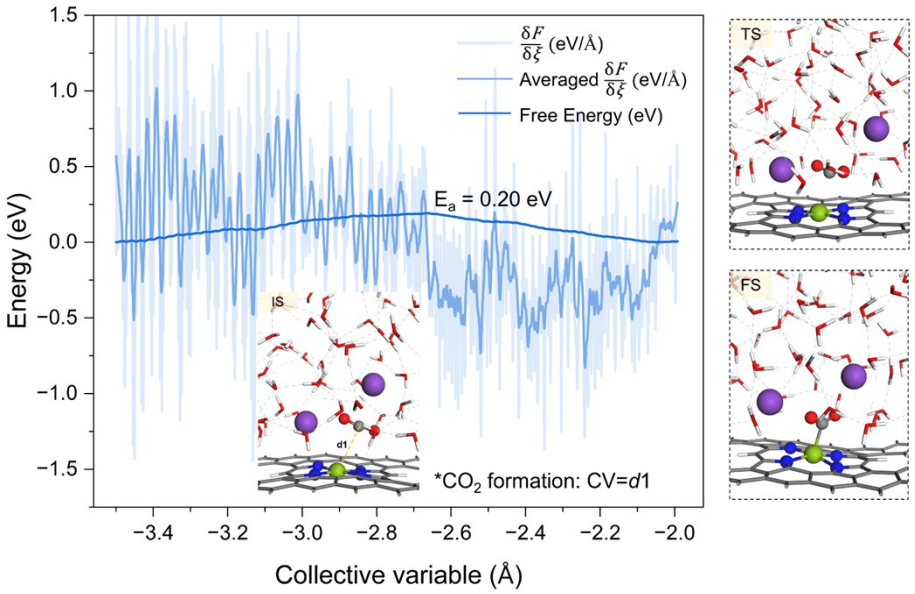

Fig. S3. Free energy profiles for CO_2 adsorption under $2K^+$ condition. The insert is the view of the initial state (IS) while the views of the transition state (TS) and final state (FS) are displayed on the right.

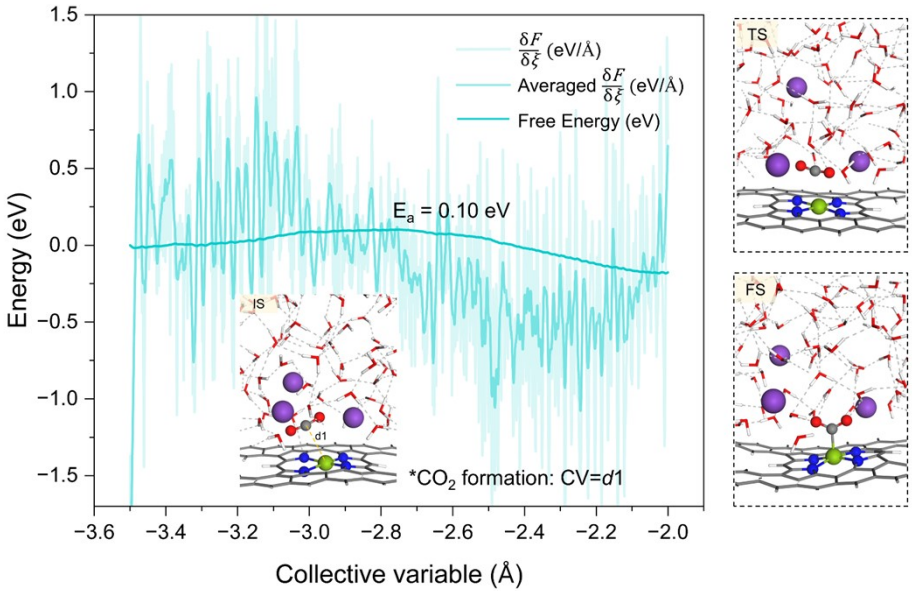

Fig. S4. Free energy profiles for CO_2 adsorption under $3K^+$ condition. The insert is the view of the initial state (IS) while the views of the transition state (TS) and final state (FS) are displayed on the right.

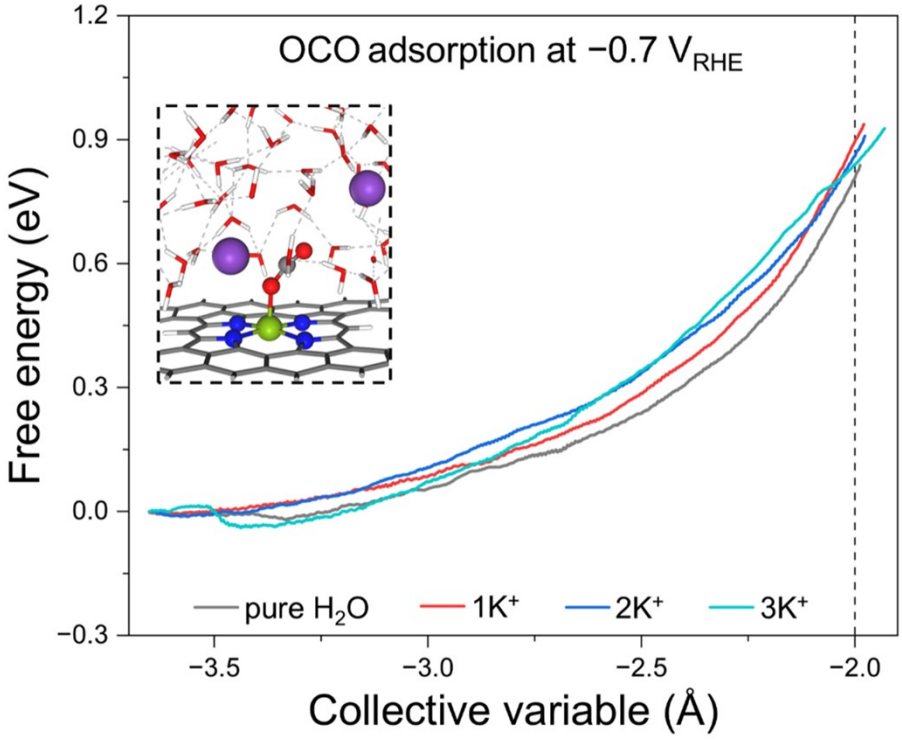

Fig. S5. Free energy profiles for CO_2 adsorption over Ni-N-C SACs under different K^+ conditions.

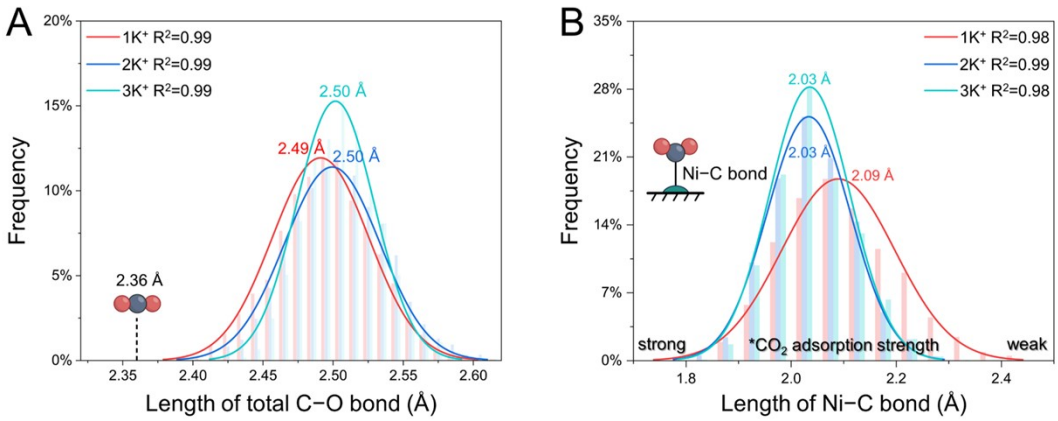

Fig. S6. Statistical analysis for the distribution of (A) the length of total C−O bond and (B) the length of Ni−C bond under three K^+ conditions.

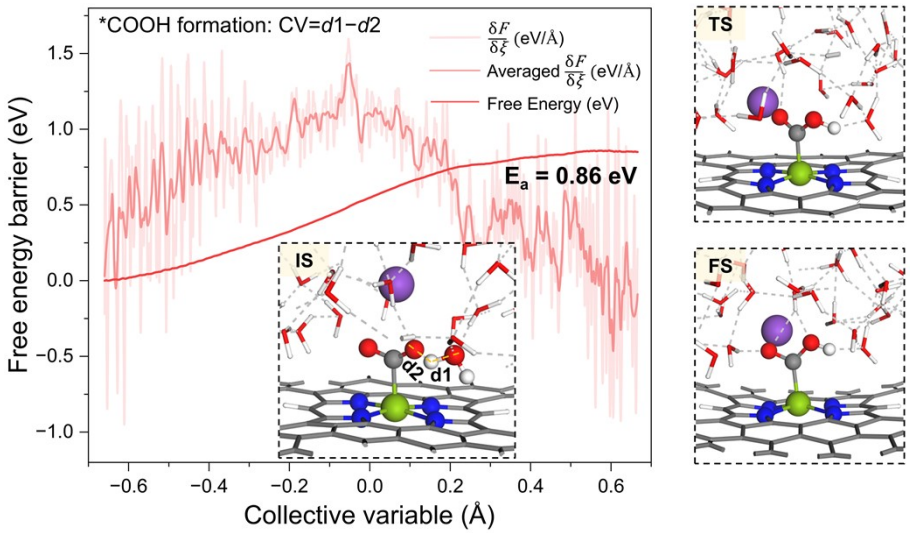

Fig. S7. Free energy profiles for *COOH formation under $1K^+$ condition. The insert is the view of the initial state (IS) while the views of the transition state (TS) and final state (FS) are displayed on the right.

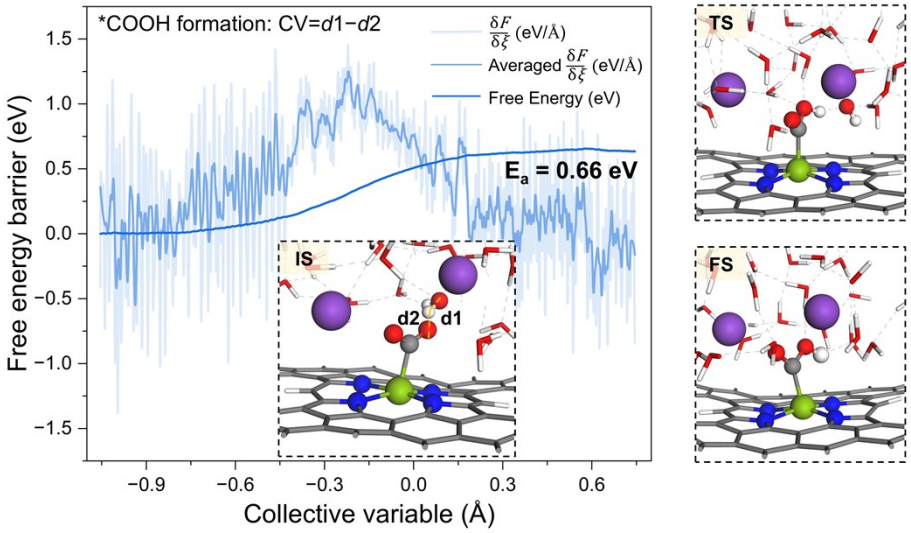

Fig. S8. Free energy profiles for *COOH formation under $2K^+$ condition. The insert is the view of the initial state (IS) while the views of the transition state (TS) and final state (FS) are displayed on the right.

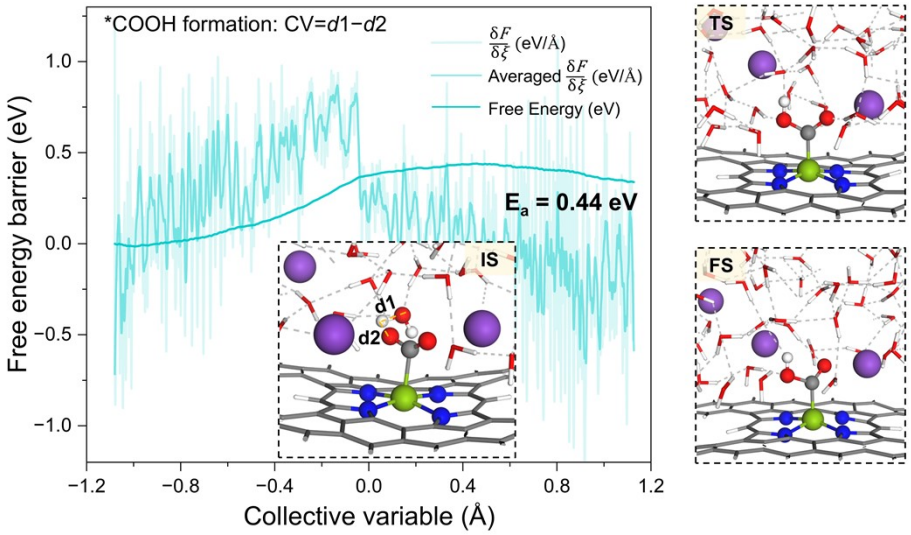

Fig. S9. Free energy profiles for *COOH formation under $3K^+$ condition. The insert is the view of the initial state (IS) while the views of the transition state (TS) and final state (FS) are displayed on the right.

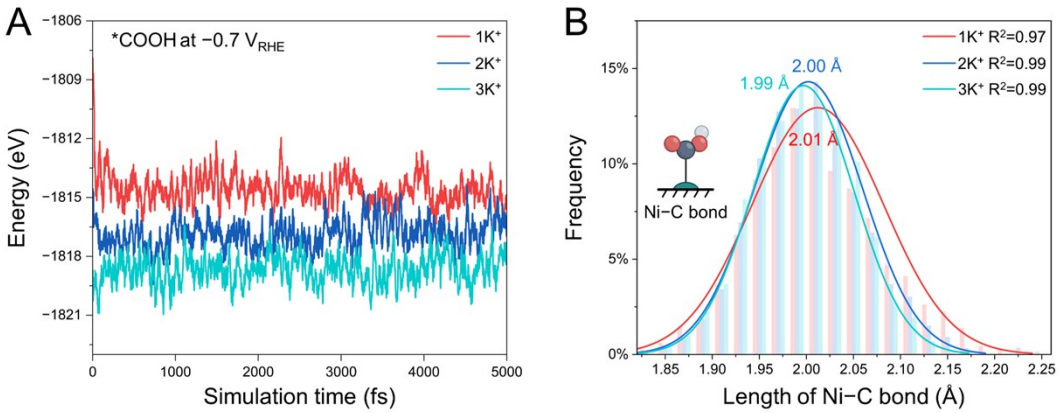

Fig. S10. (A) Variations of energy against the time during the constant-potential AIMD simulations for *COOH adsorption on Ni-N-C SACs at −0.7 V_{RHE}. (B) Statistical analysis for the distribution of the length of Ni-C bond with three interfacial cation concentrations.

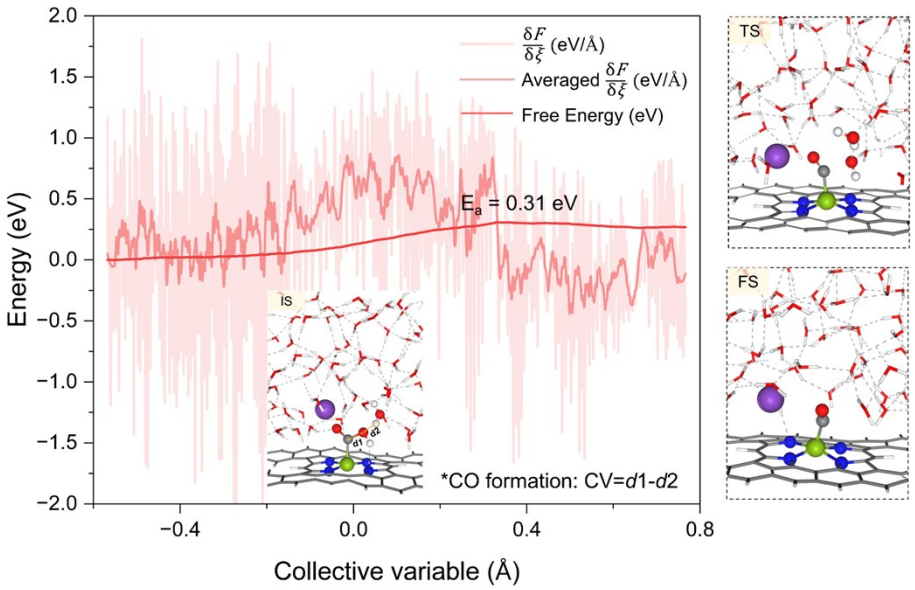

Fig. S11. Free energy profiles for *CO formation under $1K^+$ condition. The insert is the view of the initial state (IS) while the views of the transition state (TS) and final state (FS) are displayed on the right.

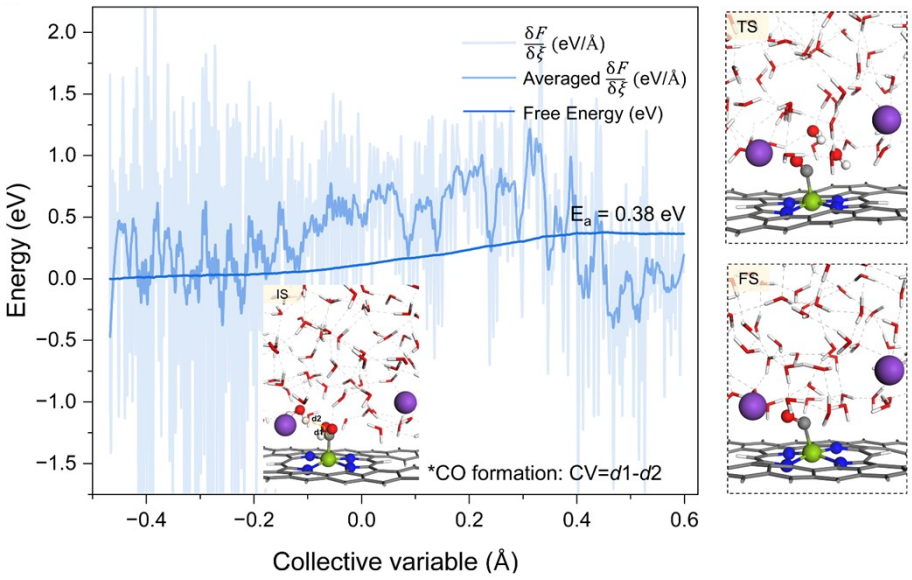

Fig. S12. Free energy profiles for *CO formation under $2K^+$ condition. The insert is the view of the initial state (IS) while the views of the transition state (TS) and final state (FS) are displayed on the right.

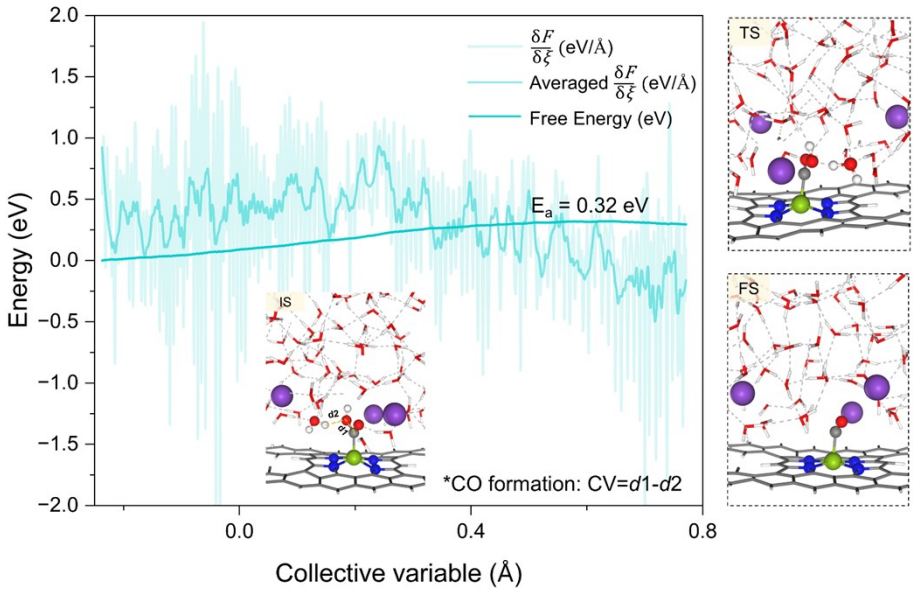

Fig. S13. Free energy profiles for *CO formation under $3K^+$ condition. The insert is the view of the initial state (IS) while the views of the transition state (TS) and final state (FS) are displayed on the right.

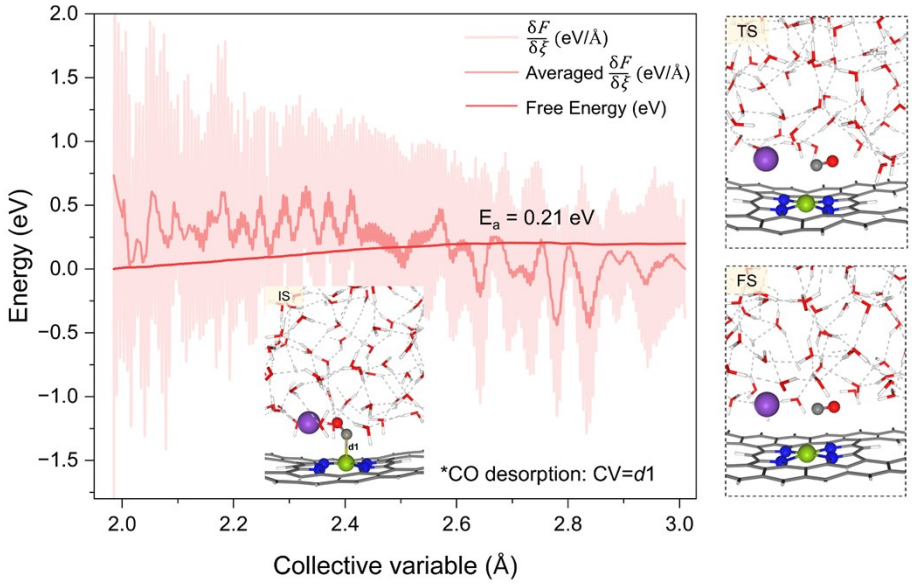

Fig. S14. Free energy profiles for *CO desorption under $1K^+$ condition. The insert is the view of the initial state (IS) while the views of the transition state (TS) and final state (FS) are displayed on the right.

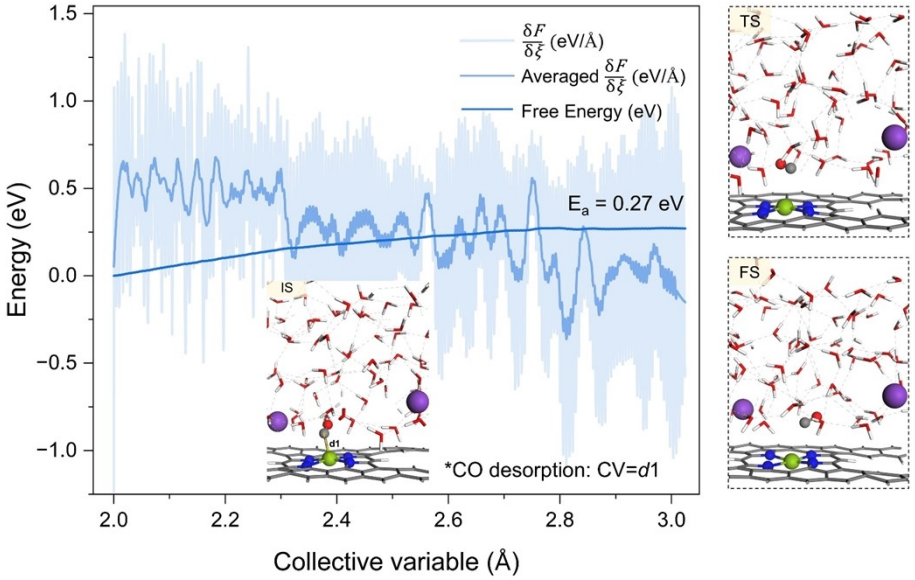

Fig. S15. Free energy profiles for *CO desorption under $2K^+$ condition. The insert is the view of the initial state (IS) while the views of the transition state (TS) and final state (FS) are displayed on the right.

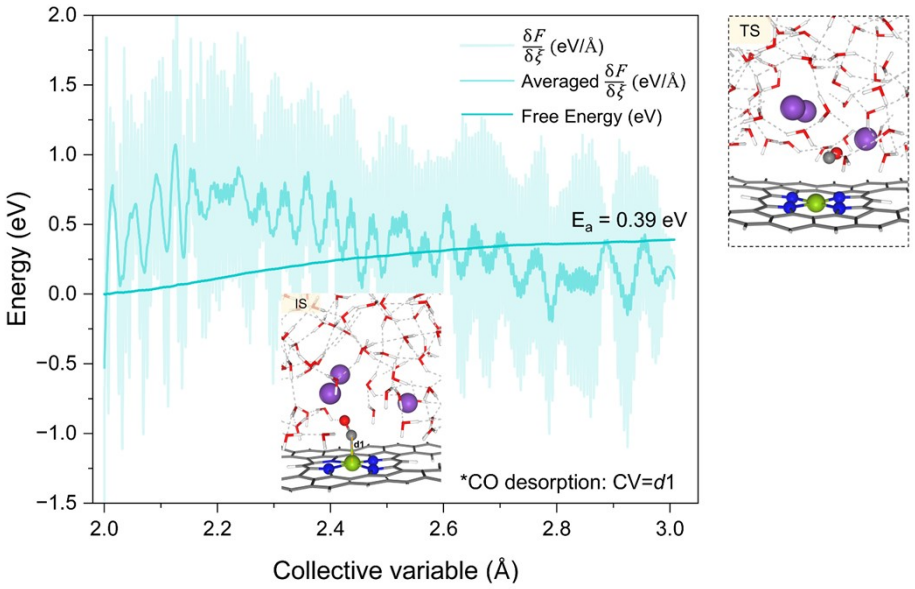

Fig. S16. Free energy profiles for *CO desorption under $3K^+$ condition. The insert is the view of the initial state (IS) while the view of the transition state (TS) is displayed on the right.

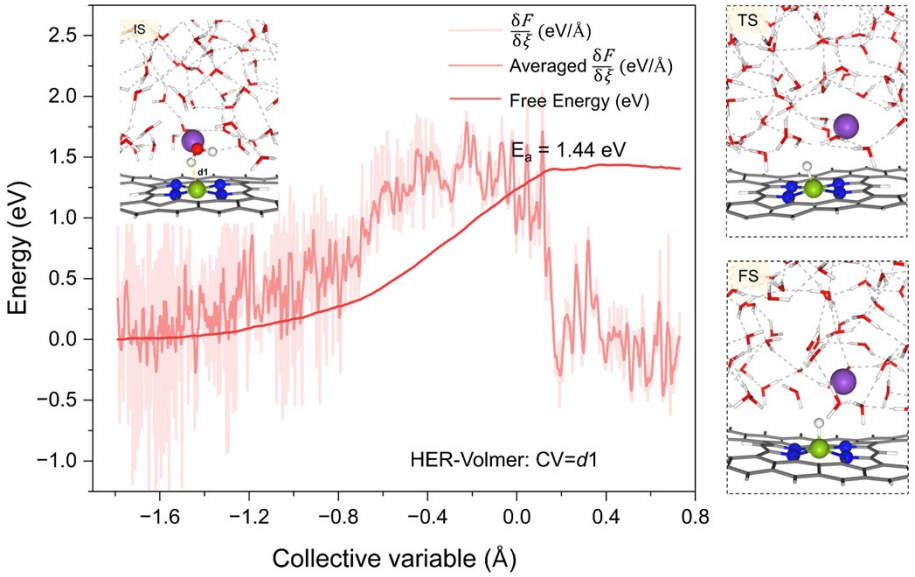

Fig. S17. Free energy profiles for *H adsorption under $1K^+$ condition. The insert is the view of the initial state (IS) while the views of the transition state (TS) and final state (FS) are displayed on the right.

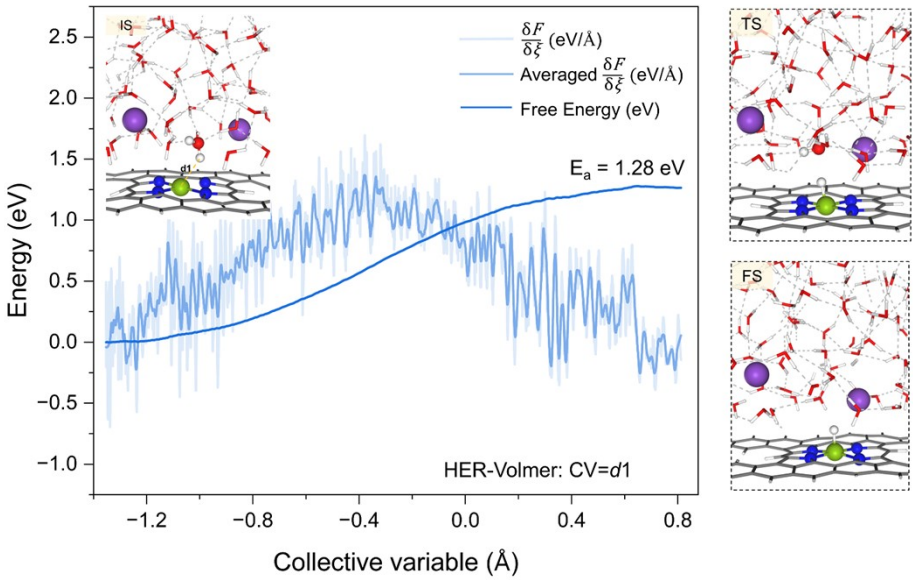

Fig. S18. Free energy profiles for *H adsorption under $2K^{+}$ condition. The insert is the view of the initial state (IS) while the views of the transition state (TS) and final state (FS) are displayed on the right.

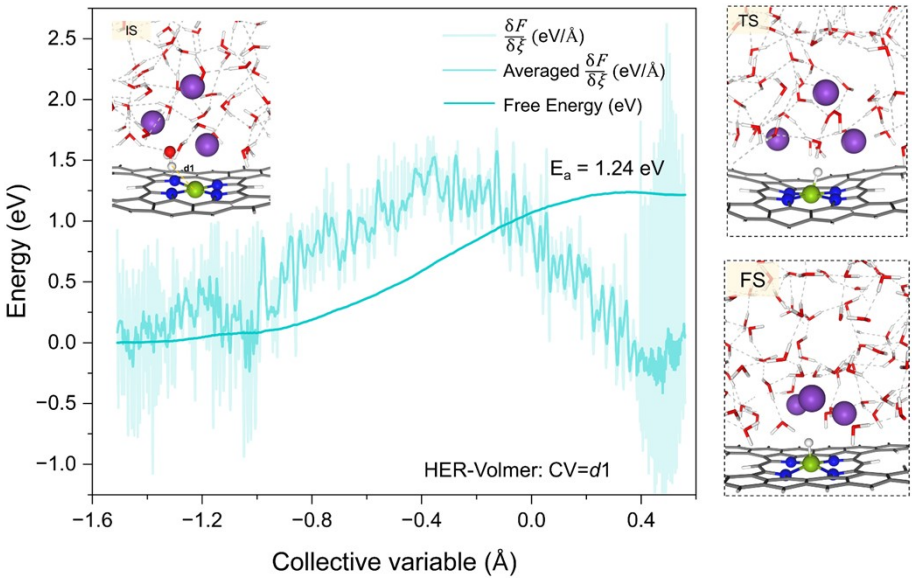

Fig. S19. Free energy profiles for *H adsorption under $3K^{+}$ condition. The insert is the view of the initial state (IS) while the views of the transition state (TS) and final state (FS) are displayed on the right.

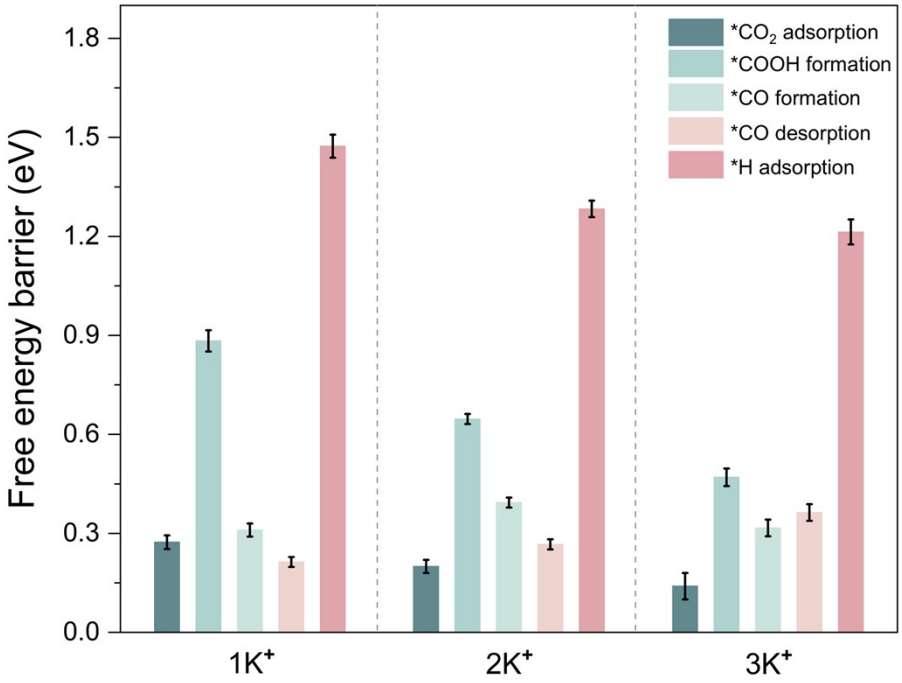

Fig. S20. Error bars representing the kinetic barriers of the key process of CO_2RR at different cation concentrations.

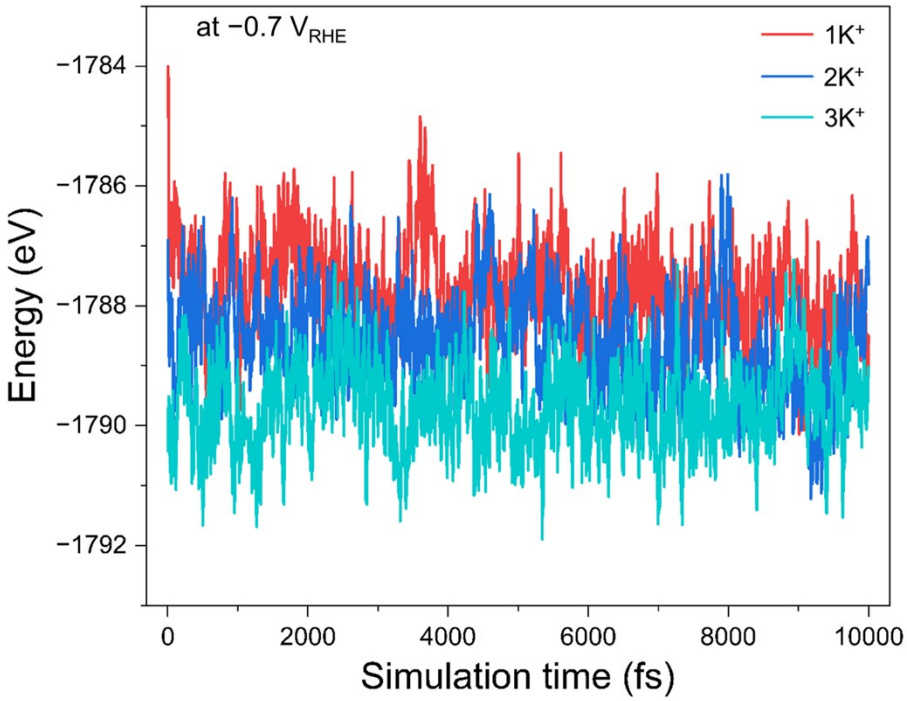

Fig. S21. Variations of energy against the time during the constant-potential AIMD simulations on Ni-N-C SACs at −0.7 V_{RHE}.

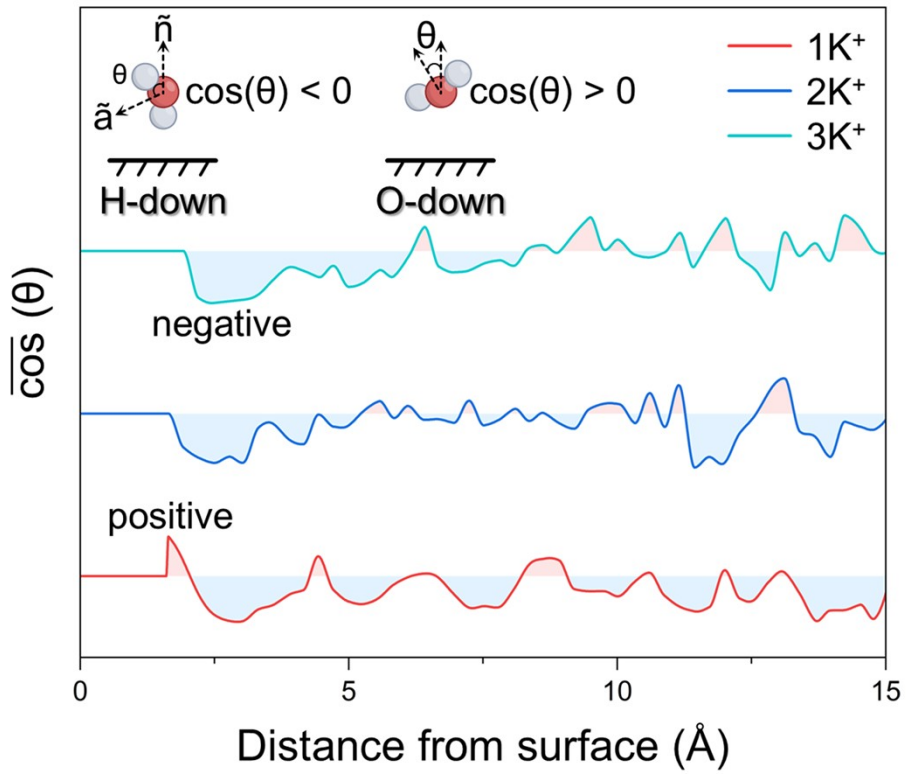

Fig. S22. Orientation of interfacial H_2O molecules. Distribution profiles of the angle (ϕ) between the water angle bisector (ã) and the surface normal (ñ).

The orientation of the explicit H_2O molecules was analyzed by geometrically summarizing the cosine function of the angle (ϕ) between the water angle bisector (ã) and the surface normal (ñ) in the AIMD trajectories. Specifically, the positive value of cos(ϕ) corresponds to the "O-down" orientation, while the "H-down" orientation is represented by the negative value of cos(ϕ). In this case, the orientation of the explicit electrolyte can be quantitatively described by calculating the average value of cos(ϕ) along the z direction. In the $1K^+$ environment, a positive peak was observed near the catalytic surface, indicating that interfacial H_2O molecules are predominantly in the "O-down" orientation. In contrast, this peak shifts to the negative side in the $2K^+$ and $3K^+$ environments, implying that at higher cation concentrations, interfacial H_2O molecules with the "H-down" orientation become dominant.

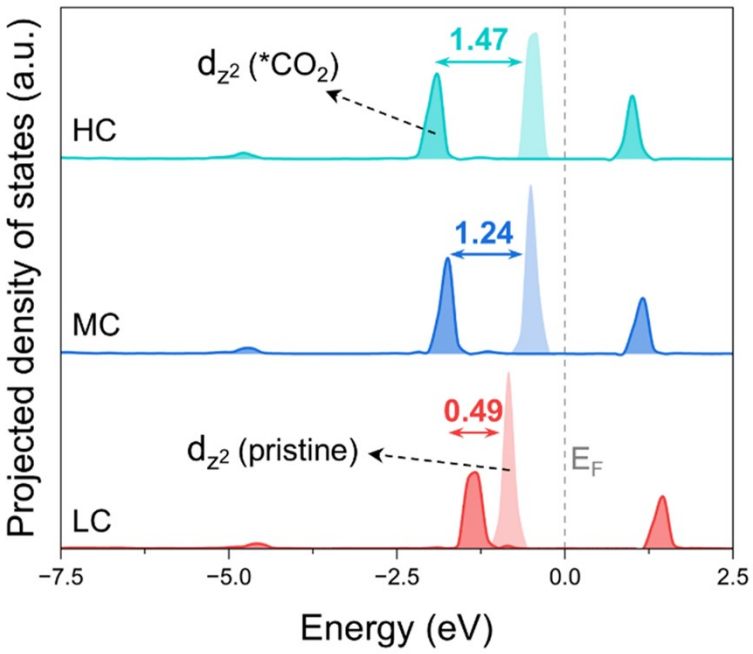

Fig. S23. Projected density of states of Ni-d_{z2} before and after CO_2 adsorption. The Fermi level (E_F) was set to zero.

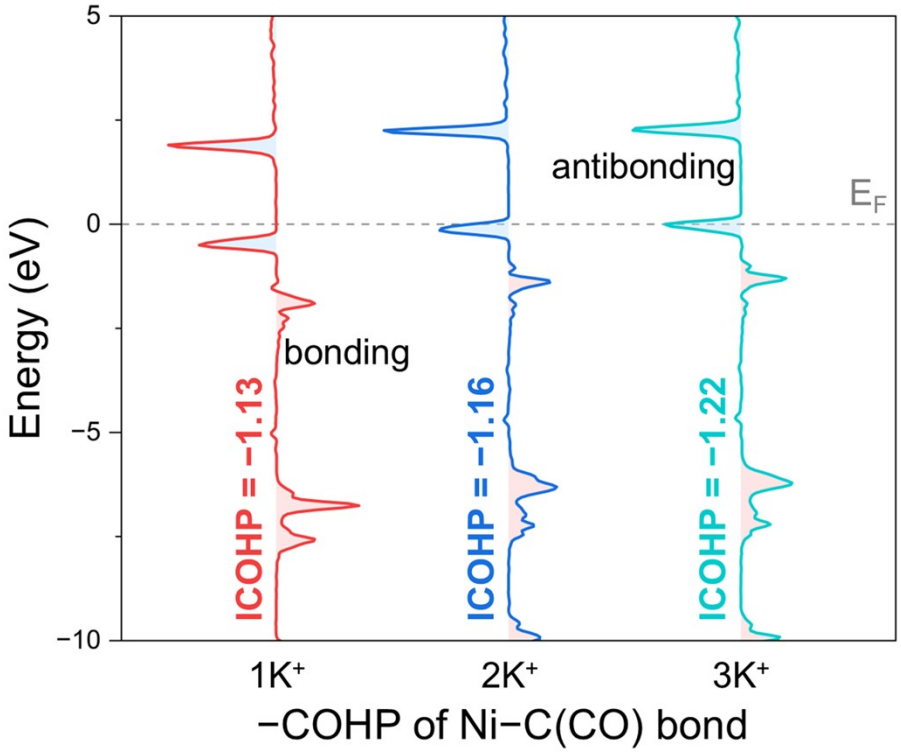

Fig. S24. COHP of the Ni-C (*CO) bond under different interfacial conditions. The Fermi level (E_F) was set to zero, with bonding and antibonding states shown on the right and left, respectively.

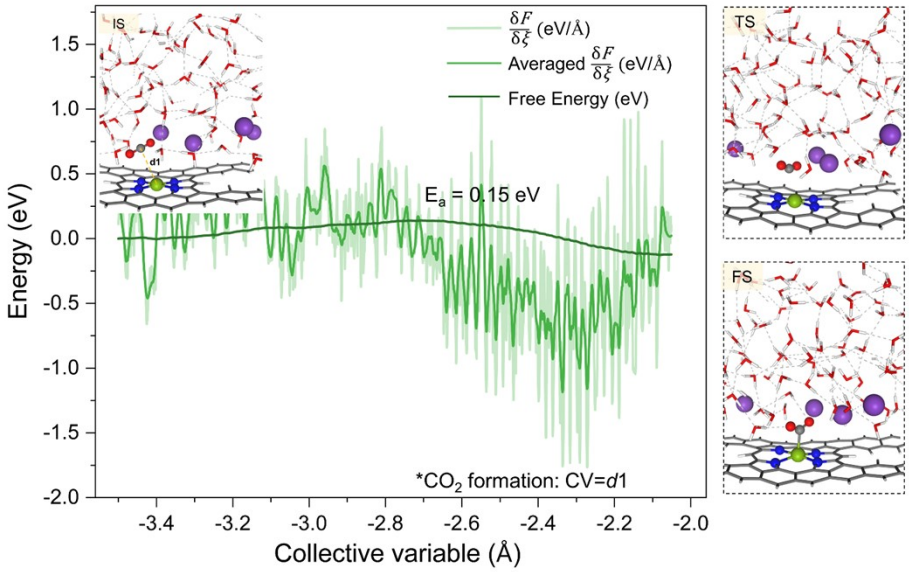

Fig. S25. Free energy profiles for $^*CO_2$ adsorption under $4K^+$ condition. The insert is the view of the initial state (IS) while the views of the transition state (TS) and final state (FS) are displayed on the right.

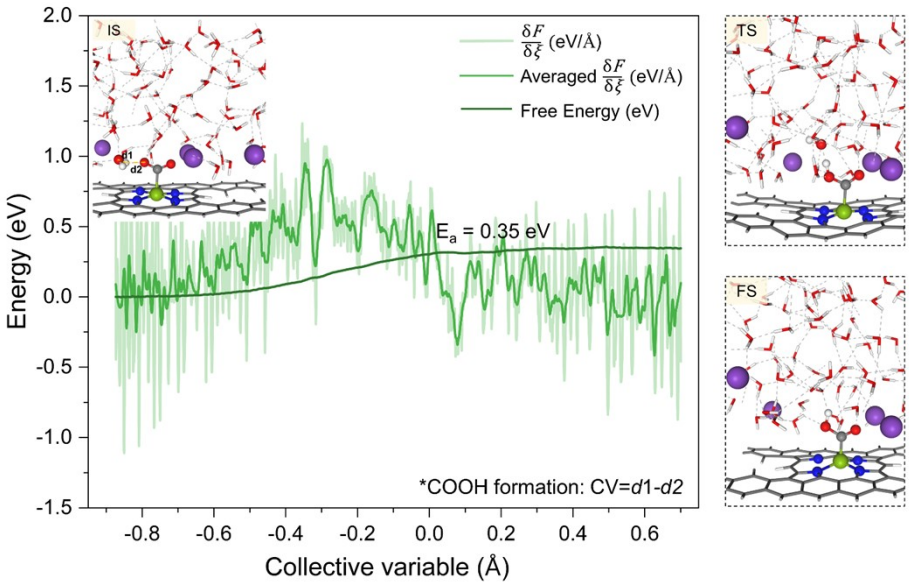

Fig. S26. Free energy profiles for *COOH formation under $4K^+$ condition. The insert is the view of the initial state (IS) while the views of the transition state (TS) and final state (FS) are displayed on the right.

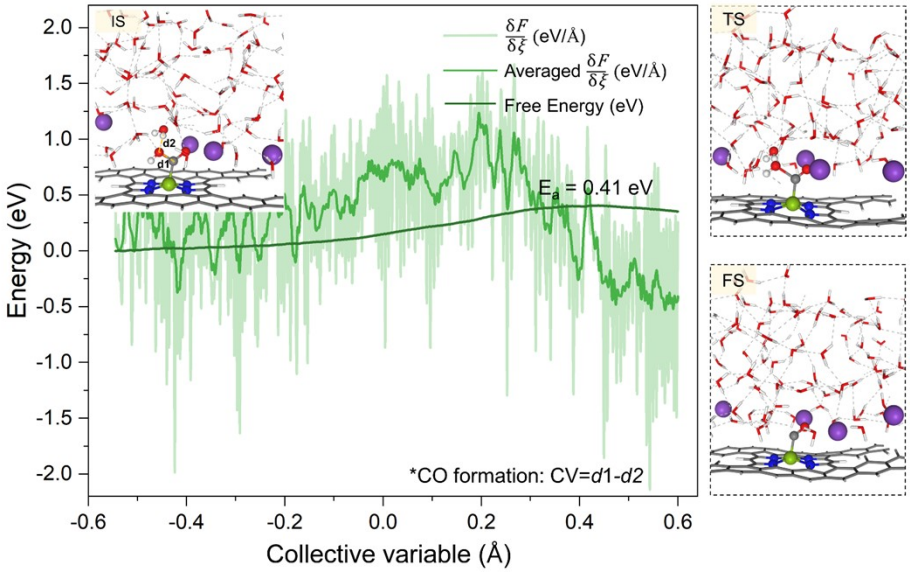

Fig. S27. Free energy profiles for *CO formation under $4K^{+}$ condition. The insert is the view of the initial state (IS) while the views of the transition state (TS) and final state (FS) are displayed on the right.

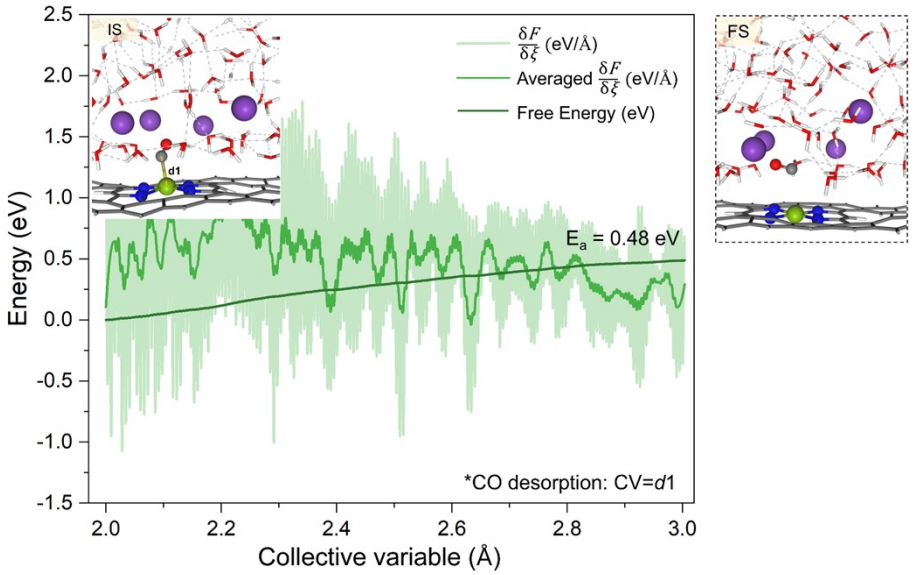

Fig. S28. Free energy profiles for *CO desorption under $4K^+$ condition. The insert is the view of the initial state (IS) while the views of the transition state (TS) and final state (FS) are displayed on the right.

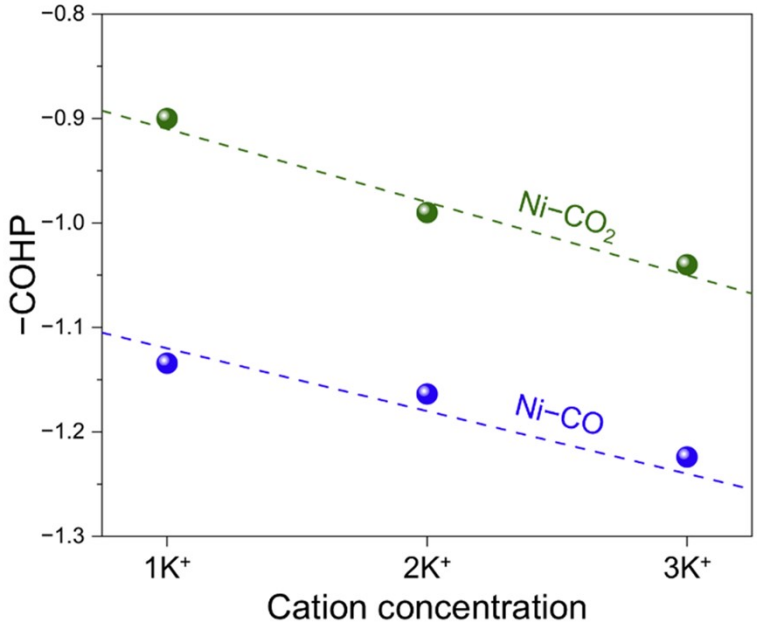

Fig. S29. Relationship between ICOHP value and cation concentration.

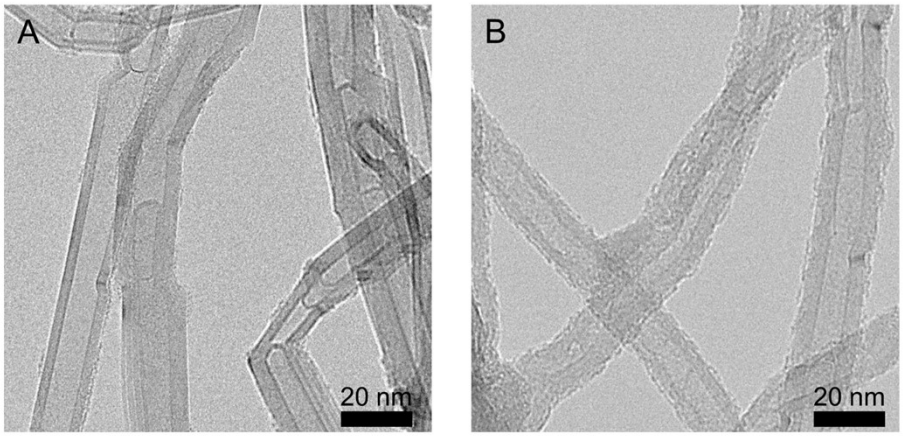

Fig. S30. TEM images of (a) pre-treated CNTs and (b) Ni-$N_{pyrrolic}$@CNT.

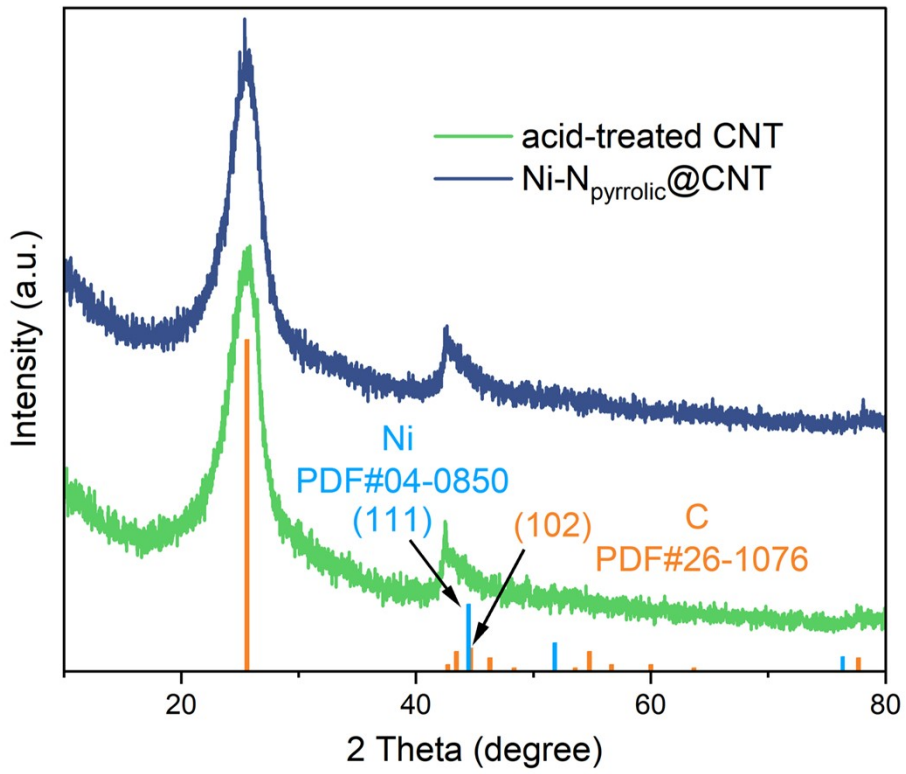

Fig. S31. X-ray diffraction (XRD) patterns of acid-treated CNT and Ni-$N_{pyrrolic}$@CNT.

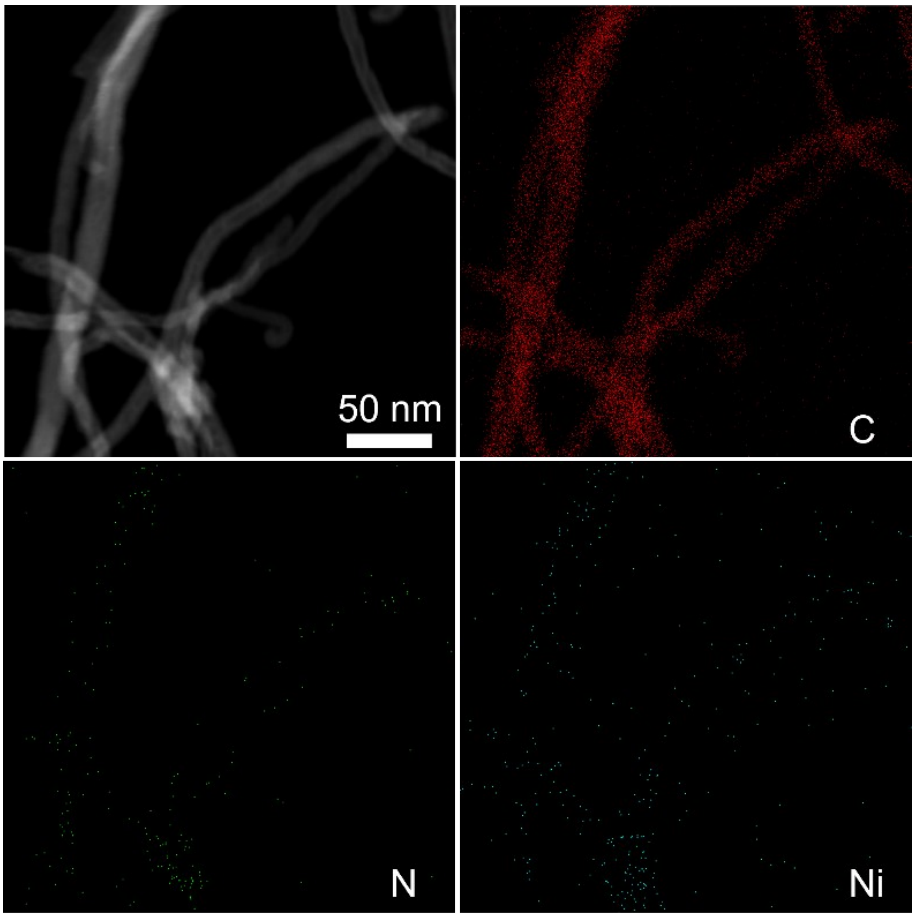

Fig. S32. HAADF-STEM image and the corresponding EDS elemental maps of Ni-$N_{pyrrolic}$@CNT.

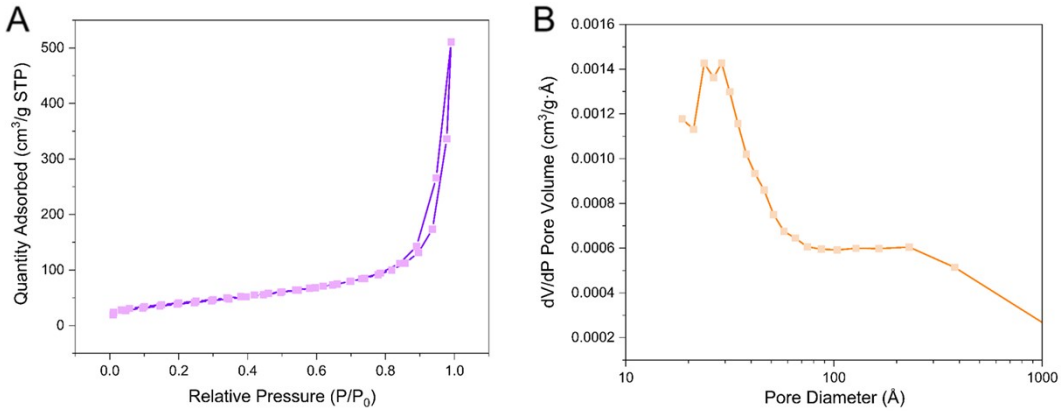

Fig. S33. (A) BET surface area analysis of Ni-$N_{pyrrolic}$@CNT; (B) Pore size distribution of Ni-$N_{pyrrolic}$@CNT.

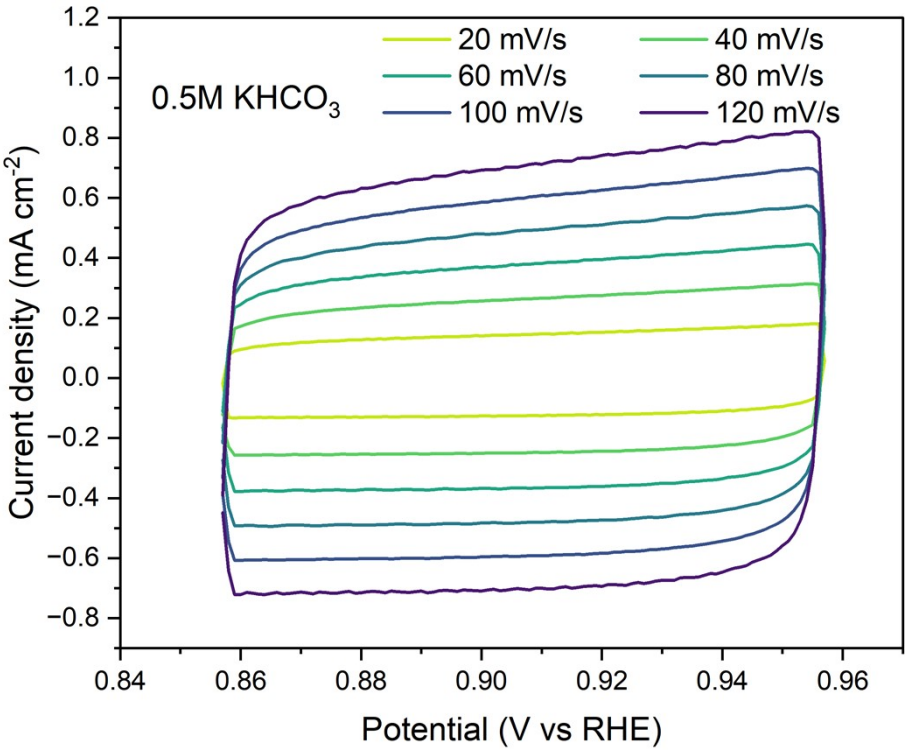

Fig. S34. CV curves at different scanning rates (20, 40, 60, 80, 100, 120 mV/s).

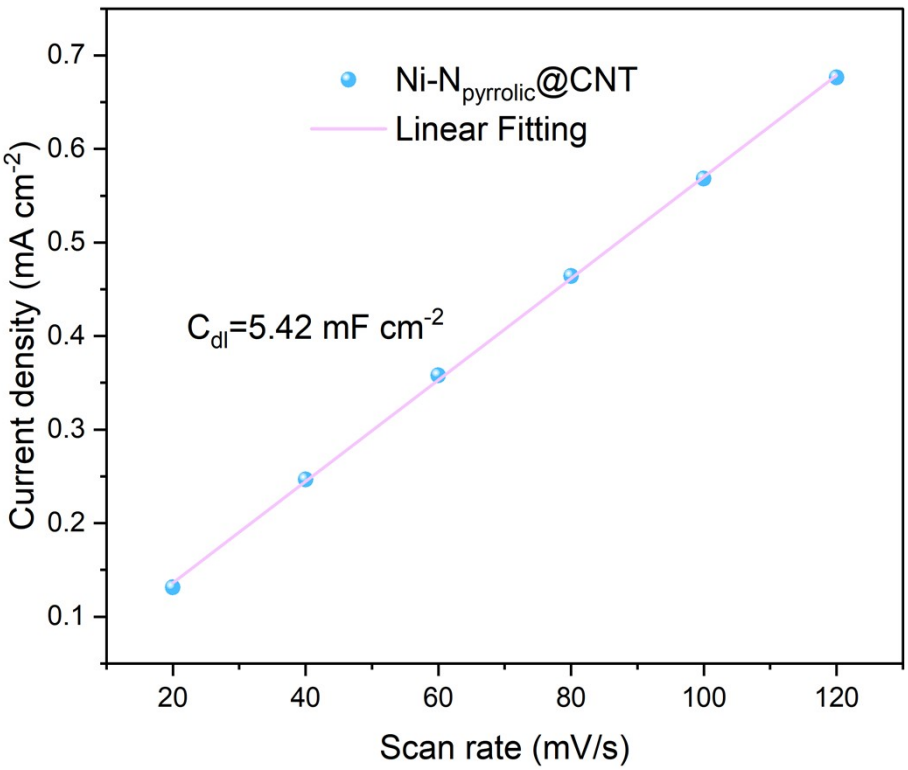

Fig. S35. Double-layer capacitor (C_{dl}) of Ni-$N_{pyrrolic}$@CNT.